Detuned square ring resonators for multiple plasmon-induced transparencies in metal–insulator–metal waveguide

2015 Appl. Phys. Express 8 112201

(http://iopscience.iop.org/1882-0786/8/11/112201)

Applied Physics Express **8**, 112201 (2015)
http://dx.doi.org/**10.7567/APEX.8.112201**

Detuned square ring resonators for multiple plasmon-induced transparencies in metal–insulator–metal waveguide

Xinru Shen[1,2], Yueke Wang[1,2*], Quansheng Chen[1,2], and Xinyu Wu[1,2]

[1]*Optical Information Science and Technology Department, Jiangnan University, Wuxi, Jiangsu 214122, China*
[2]*Optoelectronic Engineering and Technology Research Center, Jiangnan University, Wuxi, Jiangsu 214122, China*
E-mail: ykwang@jiangnan.edu.cn

Received August 3, 2015; accepted October 1, 2015; published online October 26, 2015

We propose a metal–insulator–metal (MIM) waveguide with two detuned square ring resonators to achieve on-chip multiple plasmon-induced transparencies (PITs). PITs can be explained by a well-defined phase coupling that can be established between detuned resonances. For third-order detuned resonances, there is one PIT window. For second-order detuned resonances, there are one, two, or three PIT windows, depending on the detuning degree between the two square ring resonators. Electromagnetic simulation based on the finite element method is carried out to calculate the PIT transmission spectrum and electromagnetic field distribution. © 2015 The Japan Society of Applied Physics

Electromagnetically induced transparency (EIT) is a coherently quantum destructive interference phenomenon[1)] between excitation pathways to an atomic upper level, which introduces a transparent region between two resonances.[2,3)] However, some experimental conditions, such as cryogenic temperature and gaseous medium, restrict the realization of EIT in atomic systems. With the development of nanofabrication technology, classical configurations with the EIT-like spectral response,[4)] such as coupled resonators[5)] and metamaterials,[6)] have become the research focus, which bring the original quantum phenomenon into the realm of classical optics.

Surface plasmon polaritons (SPPs) are waves propagating along metallic surfaces, originating from the interaction between the free electrons of metal and the electromagnetic field. SPPs' amplitude decays exponentially along with distance,[7)] and it can break the classical diffraction limit and manipulate light in the nanoscale domain.[8)] As an analogy of EIT based on SPPs, plasmon-induced transparency (PIT) in integrated plasmonics is of special interest for high-intensity photonic integration owing to the possibility of realizing devices with an ultrasmall footprint.[9)] In general, the PIT effect can be divided into two categories according to two different physical pictures. In one picture, PIT is achieved by a well-defined phase coupling that can be established between detuned resonances.[10)] In the other picture, PIT arises from the normal-mode splitting of a low-Q (radiative) resonance induced by its coupling with a high-Q (dark) resonance.[11)] There are various types of application based on PIT, such as slow light devices,[12)] biosensing,[13)] plasmonic switching,[14)] and plasmon rulers,[15)] which attribute to the special dispersion and transmission around the transparency window. Recently, the on-chip PIT effect in the metal–insulator–metal (MIM) waveguide, which is the analogy of the on-chip EIT, has been widely investigated. Zhang et al. introduced EIT-like phenomena using a plasmonic waveguide configuration with a comb line slot,[16)] and Han and Bozhevolnyi introduced two detuned Fabry–Perot resonators aperture-side-coupled to a MIM waveguide.[17)] To achieve a broad PIT window, a periodic array of two detuned resonators aperture-side-coupled to a MIM waveguide is introduced.[18,19)] Besides, the interference between multiple SPP resonators can produce more transparency windows.[20–23)] In addition, the research progress of graphene plasmonics paves an efficient way to achieve tunable EIT-like effects in infrared and far-infrared regions by tuning the gate voltages.[24–28)]

In this paper, a MIM waveguide with two detuned square ring resonators is proposed to achieve on-chip multiple PITs. There is one PIT peak due to the destructive interference between third-order detuned resonances. There are one, two, or three PIT peaks for second-order detuned resonances, depending on the detuning degree between the two square ring resonators. We used the finite element method (FEM) to verify the on-chip multiple PITs. Compared with the coupled microring resonators used in previous works,[29–31)] our proposed structures can use only two detuned square ring resonators to produce multiple PIT peaks, which can be applied to microring filters.

Before we introduce the detuned square ring resonator structure, we investigate theoretically and numerically the transmission of SPPs in a MIM waveguide with one square ring resonator (SRR). Figure 1(a) shows the structure of a MIM waveguide with one SRR. The dark-colored part is metal (here, we choose silver) and the light-colored part is air. The widths of the MIM waveguide and SRR are represented by w_1 and w_2, respectively. The outer side length of the SRR is represented by d. Besides, the distance between the bus waveguide and the SRR is $D = 40$ nm throughout this study.

The frequency-dependent dielectric constant of Ag is described using the Drude mode: $\varepsilon_m(\omega) = \varepsilon_\infty - \omega_p^2/(\omega^2 + i\omega\gamma)$. It can fit the experimental results of the silver permittivity well[32)] in the near-infrared region. Here, we set the relevant parameters as the permittivity at the infinite angular frequency (ε_∞) of 3.7, the bulk plasma frequency (ω_p) of 1.38×10^{16} rad/s, and the oscillation damping of electrons (γ) of 2.73×10^{13} rad/s. The dielectric constant of air (ε_0) is 1. Because of the MIM symmetry, the SPP mode (the fundamental transverse magnetic mode TM_0) can be excited by the end-fire method. The TM_0 mode does not exhibit a cutoff width. In this work, the insulator widths w_1 and w_2 are chosen as 30 and 50 nm, respectively, which means that only the TM_0 mode exists. The dispersion equation of the TM_0 mode is

$$\tanh\left(\frac{\sqrt{\beta_i^2 - k_0^2\varepsilon_0}\,w_i}{2}\right) = \frac{-\varepsilon_0\sqrt{\beta_i^2 - k_0^2\varepsilon_m(\omega)}}{\varepsilon_m(\omega)\sqrt{\beta_i^2 - k_0^2\varepsilon_0}}, \quad (1)$$

where β_i ($i = 1, 2$) are the propagation constants of TM_0 in the MIM waveguide and SRR, respectively, and k_0 is the wave vector of light in free space. The transmission is calculated by normalizing the power output from the left port to the incident

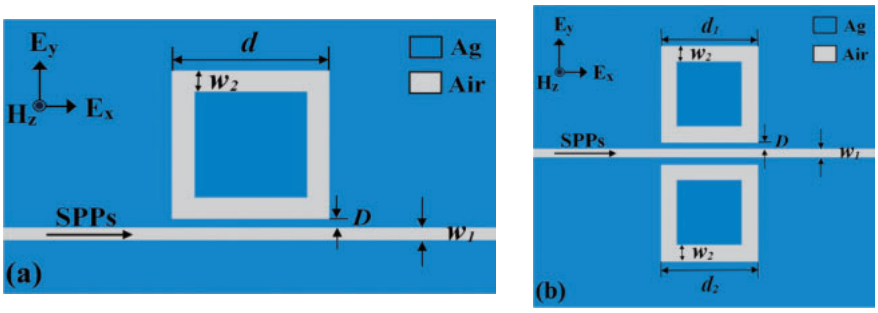

Fig. 1. Schematics of (a) a MIM waveguide with one SRR and (b) that with two SRRs.

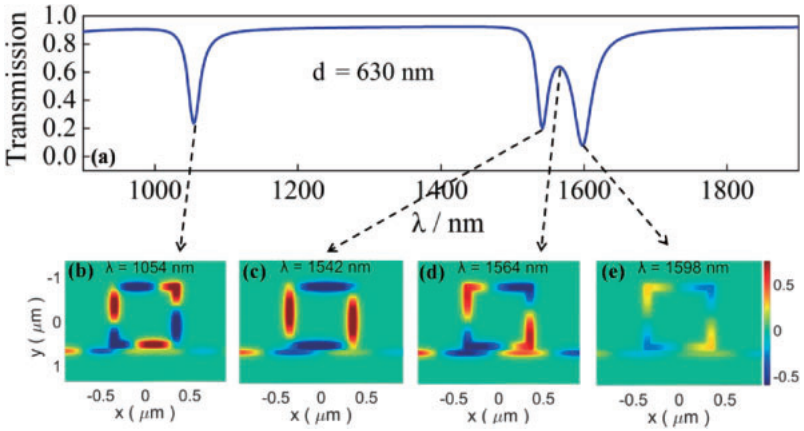

Fig. 2. (a) Transmission spectrum of a MIM waveguide with one SRR for $d = 630$ nm. Magnetic field distributions [Re(H_z)] under (b) $\lambda_0 = 1054$ nm, (c) $\lambda_0 = 1542$ nm, (d) $\lambda_0 = 1564$ nm, and (e) $\lambda_0 = 1598$ nm.

power. All the numerical simulation results here are obtained by FEM.

When the TM_0 mode propagates along the MIM waveguide from left to right, as shown in Fig. 1(a), the SPPs can be coupled to the SRR. When the SRR is in resonance, the transmission spectrum can generate a dip, and most parts of the SPPs cannot propagate to the right port of the MIM waveguide. The resonant condition of the SRR is shown as

$$4ln_{\text{eff}} = N\lambda_0. \quad (2)$$

As discussed in Ref. 33, the waveguiding length l is the average of the inner and outer perimeters of the ring, N is the resonant order, and λ_0 is the resonant wavelength. n_{eff} is the effective refractive index of the TM_0 mode in SRR, and $n_{\text{eff}} = \text{Re}(\beta_2)/k_0$.

Figure 2(a) shows the transmission spectrum in the near-infrared region for $d = 630$ nm, and there are three dips at $\lambda_0 = 1054$, 1542, and 1598 nm. Figure 2(b) shows the magnetic field distribution Re(H_z) under $\lambda_0 = 1054$ nm, which demonstrates that the ring is in third-order resonance. Figures 2(c) and 2(e) show Re(H_z) under $\lambda_0 = 1542$ and 1598 nm, which correspond to the two standing-wave modes originating from the splitting of the second-order resonance.[33] The SPP energy concentrates on the face and corner parts of the SRR for the short-wavelength (1542 nm) and long-wavelength (1598 nm) resonant modes, respectively. The reason for the mode splitting is the nonuniform distribution of n_{eff} around the SRR. Thus, one SRR in second-order resonance can be treated as two resonances. The resonant wavelengths can be approximately estimated using

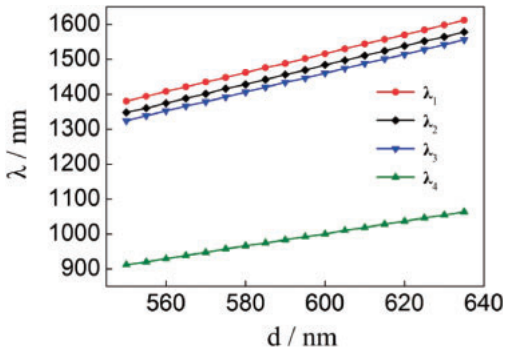

Fig. 3. Transmission dips λ_4, λ_3, and λ_1 for third- and second-order resonances, and transmission peak λ_2 between λ_3 and λ_1 with d.

Eqs. (1) and (2). Figure 2(d) shows the Re(H_z) at the transmission peak at 1564 nm. We believe that this transmission peak is not the PIT window, because it is not due to the destructive interference between detuned resonances (because there is only one SRR), but due to the splitting of the second-order resonance, as discussed in Ref. 33. There is no destructive interference for one ring structure, which violates the first PIT picture in our introduction.

For convenience, we define λ_4, λ_3, and λ_1 as the resonant wavelength for third-order resonance (TOR), the short-wavelength second-order resonance (SSOR), and the long-wavelength second-order resonance (LSOR), respectively, and λ_2 as the transmission peak between the splitting second-order modes (PSO). Figure 3 shows that λ_i ($i = 1$, 3, and 4) increases linearly with the outer side length d, which is in agreement with Eq. (2).

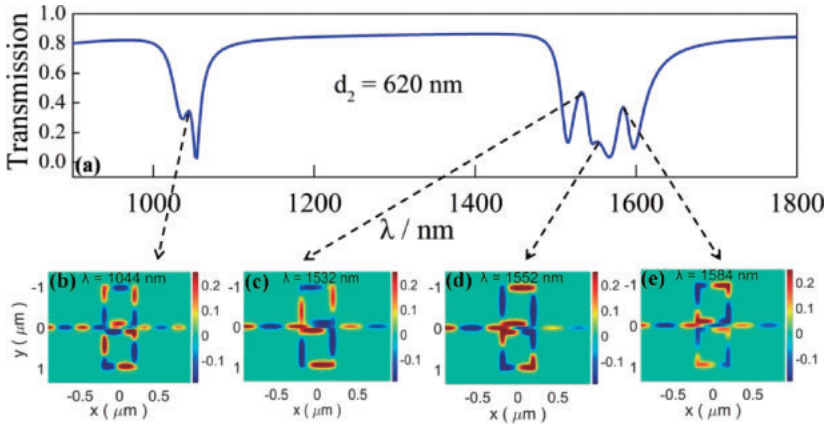

Fig. 4. (a) Transmission spectrum of a MIM waveguide with two SRRs for $d_1 = 630$ nm and $d_2 = 620$ nm. Magnetic field distributions [Re(H_z)] at PIT peaks: (b) $\lambda = 1044$ nm, (c) $\lambda = 1532$ nm, (d) $\lambda = 1552$ nm, and (e) $\lambda = 1584$ nm.

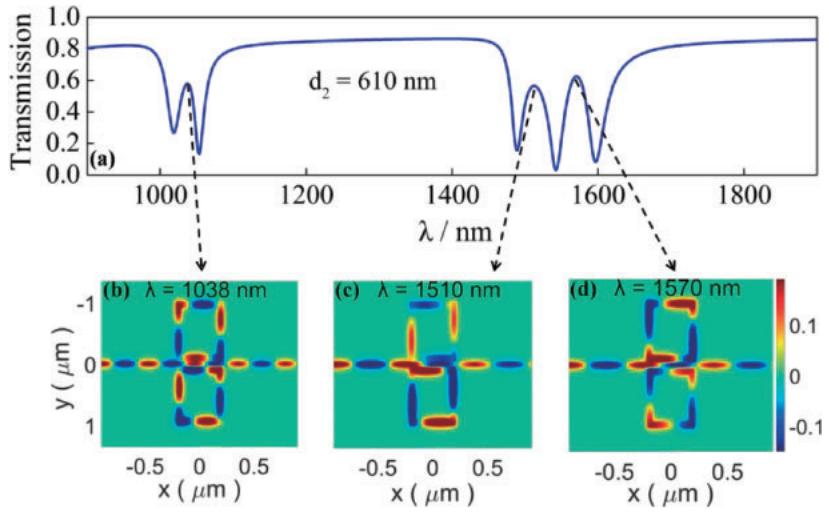

Fig. 5. (a) Transmission spectrum of a MIM waveguide with two SRRs for $d_1 = 630$ nm and $d_2 = 610$ nm. Magnetic field distributions [Re(H_z)] at PIT peaks: (b) $\lambda = 1038$ nm, (c) $\lambda = 1510$ nm, and (d) $\lambda = 1570$ nm.

On the basis of the transmission characteristics of the MIM waveguide with one SRR, we propose a MIM waveguide with two detuned SRRs to achieve multiple PITs. Figure 1(b) shows the theoretical model of the MIM waveguide with two detuned SRRs. Two SRRs with different outer side lengths d_1 and d_2 locate at the upside and downside of the MIM waveguide and are signed by SRR1 and SRR2, respectively. Other parameters are chosen to be the same as those of a MIM waveguide with one SRR. Here, d_1 is fixed to be 630 nm, and the PIT transmission spectrum with decreasing d_2 from 630 nm can be obtained. We believe that the results of the PIT transmission spectrum with increasing d_2 from 630 nm are similar and need not be discussed here.

Figure 4(a) shows the transmission spectrum under $d_2 =$ 620 nm, and there are four PIT peaks at $\lambda = 1044$, 1532, 1552, and 1584 nm. For $\lambda = 1044$ nm, the PIT originates from the destructive interference between the TOR ($\lambda_4 = 1054$ nm) of SRR1 and the TOR ($\lambda_4 = 1036$ nm) of SRR2. Figure 4(b) shows Re(H_z), and the antisymmetrical distribution of phases illustrates the destructive interference. For $\lambda = 1532$, 1552, and 1584 nm, the PIT peaks originate from the destructive interferences between the SSOR ($\lambda_3 = 1514$ nm) of SRR2 and the SSOR ($\lambda_3 = 1542$ nm) of SRR1, the LSOR ($\lambda_1 = 1570$ nm) of SRR2 and the SSOR ($\lambda_3 = 1542$ nm) of SRR1, and the LSOR ($\lambda_1 = 1570$ nm) of SRR2 and the LSOR ($\lambda_1 = 1598$ nm) of SRR1, respectively. Figures 4(c)–4(e) depict the Re(H_z) for $\lambda = 1532$, 1552, and 1584 nm to illustrate the destructive interference. From the simulation results (not all shown here), when d_2 varies from 626 to 615 nm, there is one PIT peak due to the detuning of the third-order resonances, and there are three PIT peaks due to the detuning of the second-order resonances.

When d_2 varies from 615 to 605 nm, there is one PIT peak due to the detuning of the third-order resonances, and there are two PIT peaks due to the detuning of the second-order resonances. The destructive interference between the LSOR of SRR2 and the SSOR of SRR1 does not occur because the detuning between the two resonances is too small to generate a PIT window. For example, Fig. 5(a) shows the transmission spectrum under $d_2 = 610$ nm, and there are three PIT peaks at $\lambda = 1038$, 1510, and 1570 nm. For $\lambda = 1038$ nm, the PIT peak originates from the destructive interference between the TOR ($\lambda_4 = 1054$ nm) of SRR1 and the TOR ($\lambda_4 = 1018$ nm) of SRR2. For $\lambda = 1510$ and 1570 nm, the PIT peaks originate from the destructive interferences between the SSOR ($\lambda_3 = 1488$ nm) of SRR2 and the SSOR ($\lambda_3 = 1542$ nm) of SRR1, and the LSOR ($\lambda_3 = 1544$ nm) of SRR2 and the LSOR ($\lambda_3 = 1598$ nm) of SRR1, respectively.

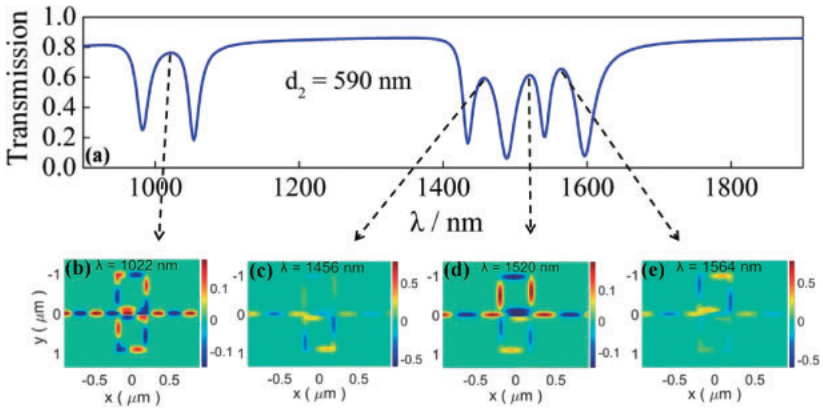

Fig. 6. (a) Transmission spectrum of a MIM waveguide with two SRRs for $d_1 = 630$ nm and $d_2 = 590$ nm. Magnetic field distributions [Re(H_z)] at (b) $\lambda = 1022$ nm, (c) $\lambda = 1456$ nm, (d) $\lambda = 1520$ nm, and (e) $\lambda = 1564$ nm.

When d_2 is shorter than 605 nm, there is one PIT peak due to the detuning of the third-order resonances of SRRs and one PIT peak due to the detuning of the second-order resonances of SRRs. The interference between the SSOR of SRR2 and the SSOR of SRR1, and that between the LSOR of SRR2 and the LSOR of SRR1 disappear because the detuning is very large. For example, Fig. 6(a) shows the transmission spectrum under $d_2 = 590$ nm, and there are two PIT peaks at $\lambda = 1022$ and 1520 nm. For $\lambda = 1022$ nm, the PIT peak originates from the destructive interference between the TOR ($\lambda_4 = 1054$ nm) of SRR1 and the TOR ($\lambda_4 = 983$ nm) of SRR2, and Fig. 6(b) depicts Re(H_z) to illustrate the destructive interference. For $\lambda = 1520$ nm, the PIT peak originates from the destructive interference between the LSOR ($\lambda_1 = 1488$ nm) of SRR2 and the SSOR ($\lambda_3 = 1542$ nm) of SRR1. The peaks located at $\lambda = 1456$ and 1564 nm are not the PIT peaks but the SSO peaks, because the peak positions and the Re(H_z) at the two peaks are the same as those of the SSO resonances shown in Fig. 3. Thus, for two detuned square ring resonators, there is one PIT peak for the third-order resonance, and there are one, two, or three PIT peaks for the second-order resonances depending on d_2. The conclusion for the third-order resonance can be extended to any odd-number-order resonance; however, the conclusion for the second-order resonance cannot be extended to any even-number-order resonance, because the splitting of the even-number-order resonance of one SRR disappears when the resonance order is larger than 6.[33)]

In conclusion, a MIM waveguide with two detuned square ring resonators is investigated theoretically and numerically. The destructive interference between third-order detuned resonances only generates one PIT window, but that between second-order detuned resonances generates multiple PIT windows. The number of PIT windows varies from one to three, when the detuning degree between the second-order resonators is increased. We believe that the proposed configurations may find significant applications in wavelength division demultiplexing systems, sensors, and slow light devices.

Acknowledgments This project was supported by the National Natural Science Foundation of China under Grant No. 11404143, the Returned Overseas Fund of the Ministry of Education of China under Grant No. 1144130201150080, and the Fundamental Research Funds for the Central Universities (JUSRP51517).

1) E. Ozbay, Science **311**, 189 (2006).
2) M. Fleischhauer, A. Imamoglu, and J. P. Marangos, Rev. Mod. Phys. **77**, 633 (2005).
3) I. Novikova, R. L. Walsworth, and Y. Xiao, Laser Photonics Rev. **6**, 333 (2012).
4) N. Papasimakis, V. A. Fedotov, N. I. Zheludev, and S. L. Prosvirnin, Phys. Rev. Lett. **101**, 253903 (2008).
5) D. Smith, H. Chang, K. A. Fuller, A. Rosenberger, and R. W. Boyd, Phys. Rev. A **69**, 063804 (2004).
6) S. Zhang, D. A. Genov, Y. Wang, M. Liu, and X. Zhang, Phys. Rev. Lett. **101**, 047401 (2008).
7) H. Raether, *Surface Plasmons on Smooth and Rough Surfaces and on Gratings* (Springer, Berlin, 1988) Springer Tracts in Modern Physics, Vol. 111.
8) Z. H. Han and S. I. Bozhevolnyi, Rep. Prog. Phys. **76**, 016402 (2013).
9) Z. Han, C. E. Garcia-Ortiz, I. P. Radko, and S. I. Bozhevolnyi, Opt. Lett. **38**, 875 (2013).
10) R. Singh, C. Rockstuhl, F. Lederer, and W. Zhang, Phys. Rev. B **79**, 085111 (2009).
11) B. Yun, G. Hu, R. Zhang, and Y. Cui, Opt. Express **22**, 28662 (2014).
12) C. Wu, A. B. Khanikaev, and G. Shvets, Phys. Rev. Lett. **106**, 107403 (2011).
13) J. F. O'Hara, R. Singh, I. Brener, E. Smirnova, J. G. Han, A. J. Taylor, and W. L. Zhang, Opt. Express **16**, 1786 (2008).
14) W.-S. Chang, J. B. Lassiter, P. Swanglap, H. Sobhani, S. Khatua, P. Nordlander, N. J. Halas, and S. Link, Nano Lett. **12**, 4977 (2012).
15) N. Liu, M. Hentschel, T. Weiss, A. P. Alivisatos, and H. Giessen, Science **332**, 1407 (2011).
16) Z. R. Zhang, L. W. Zhang, H. Q. Li, and H. Chen, Appl. Phys. Lett. **104**, 231114 (2014).
17) Z. Han and S. I. Bozhevolnyi, Opt. Express **19**, 3251 (2011).
18) Y. Huang, C. Min, and G. Veronis, Appl. Phys. Lett. **99**, 143117 (2011).
19) G. Wang, H. Lu, and X. Liu, Opt. Express **20**, 20902 (2012).
20) X. Y. Yang, X. Y. Hu, Z. Chai, C. C. Lu, H. Yang, and Q. H. Gong, Appl. Phys. Lett. **104**, 221114 (2014).
21) C. Zeng, Appl. Opt. **53**, 38 (2014).
22) H. Lu, X. M. Liu, G. X. Wang, and D. Mao, Nanotechnology **23**, 444003 (2012).
23) J. Guo, Appl. Opt. **53**, 1604 (2014).
24) L. Wang, W. Li, and X. Y. Jiang, Opt. Lett. **40**, 2325 (2015).
25) C. Zeng, Y. D. Cui, and X. M. Liu, Opt. Express **23**, 545 (2015).
26) J. Ding, B. Arigong, H. Ren, M. Zhou, J. Shao, M. Lu, Y. Chai, Y. K. Lin, and H. L. Zhang, Sci. Rep. **4**, 6128 (2014).
27) D. J. Meng, S. Y. Wang, X. L. Sun, R. Z. Gong, and C. H. Chen, Appl. Phys. Lett. **104**, 261902 (2014).
28) X. Y. Duan, S. Q. Chen, H. Cheng, Z. C. Li, and J. G. Tian, Opt. Lett. **38**, 483 (2013).
29) S. T. Chu, B. E. Little, W. G. Pan, T. Kaneko, S. Sato, and Y. Kokubun, IEEE Photonics Technol. Lett. **11**, 691 (1999).
30) T. Naganawa, S. Ueno, and Y. Kokubun, IEEE Photonics Technol. Lett. **17**, 2104 (2005).
31) Y. Hatakeyama, T. Hanai, S. Suzuki, and Y. Kokubun, IEEE Photonics Technol. Lett. **16**, 473 (2004).
32) P. B. Johnson and R. W. Christy, Phys. Rev. B **6**, 4370 (1972).
33) A. Hosseini and Y. Massoud, Appl. Phys. Lett. **90**, 181102 (2007).